Numerical investigations of cavity-soliton distillation in Kerr resonators using the nonlinear Fourier transform

Jianxing Pan,[1,*] Tianye Huang,[1,2,*] Yutian Wang,[2,3] Zhichao Wu,[1,†] Jing Zhang,[1] and Luming Zhao[2,3]
[1]*School of Mechanical Engineering and Electronic Information, China University of Geosciences, Wuhan 430074, China*
[2]*Wuhan National Laboratory Optoelectronics, Wuhan 430074, China*
[3]*School of Optical and Electronic Information, Huazhong University of Science and Technology, Wuhan 430074, China*

(Received 24 July 2021; accepted 29 September 2021; published 8 October 2021)

Dissipative cavity solitons (CSs) in a Kerr resonator have wide applications from optical communications to spectroscopy due to their broad bandwidth. Although the broadband spectrum ultrashort pulses are easy to be generated in a high-Q microresonator, such kinds of solitons in the macroscopic fiber ring resonator are difficult to be obtained. Dispersion management can be a feasible method to realize soliton compression, but the Kelly-like sidebands in the frequency domain are increased inside the cavity. To achieve a perfect soliton from a macroscopic cavity, an ingenious method of nonlinear Fourier transform (NFT) is utilized here to filter out the sidebands. The CS is mapped to different components in the nonlinear spectrum and a pure soliton can be reconstructed from the resonant continuous-wave background accordingly. Numerical simulations demonstrate NFT can be an effective method for CS analysis both in the time and frequency domains. Our investigations exemplify another application of NFT in a dissipative nonlinear system.

DOI: 10.1103/PhysRevA.104.043507

I. INTRODUCTION

Dissipative cavity solitons (CSs), sustained by the coherently driven passive Kerr resonators, have aroused considerable attention over the past few years [1–3]. Since first experimentally demonstrated in the macroscopic fiber optical resonators for achieving an all-optical buffer [4], CSs have been vigorously developed in the monolithic microresonators with smaller footprints [5,6]. Essential for the existence of bright CSs is the double balance between the Kerr nonlinearity and anomalous group-velocity dispersion (GVD), as well as periodic coherent driving and total losses. Once a soliton emerges and sits atop the continuous-wave (CW) background, it can maintain its pulse shape (amplitude and pulse width) during the propagation inside the cavity. Due to the periodic output of temporal pulses, the spectrum of CSs displays a series of discrete frequency lines with equal separation, which is usually called frequency comb [1] together with the central CW. Thus the CSs have wide applications in high-speed optical coherent communications [7], optical ranging [8,9], microwave generation [10,11], astrocombs generation [12,13], spectroscopy [14,15], etc. Compared to the ultrashort pulse corresponding to a broadband comb in the high-Q microresonators, CSs in the macroscopic fiber resonator (low Q) show low amplitude and wide pulse width (narrow spectrum). In mode-locked fiber lasers, to shorten the pulse width and enhance the pulse energy, dispersion management of the cavity has been widely exploited [16,17]. Similar to the fiber lasers, dispersion management has been theoretically and experimentally adopted in the passive Kerr resonators [18,19]. By stretching and compressing twice in a single round-trip propagation inside the cavity, the amplitude of CSs and the bandwidth of their spectrum are increased. However, CSs circulated in the dispersion-managed cavity are perturbed to radiate strong sidebands on the spectrum [20], which are known to be Kelly-like sidebands as those in fiber lasers [21]. These sidebands coherently interfering with CSs decrease the smoothness of the spectrum. Therefore, how to filter out these sidebands and recover a pure soliton (PS) could be a key point for specific applications.

Recently, differing from the traditional Fourier transform method, a novel spectrum analysis method has been applied to investigate the characteristics of solitons in the mode-locked lasers [22–25] and the passive resonators [26], which is called nonlinear Fourier transform (NFT). Originally proposed for solving certain nonlinear dispersive partial differential equations [27], NFT is soon after associated with the notion of solitons in integrable models such as nonlinear Schrödinger equations (NLSEs) [28]. The temporal pulses can be projected onto the nonlinear spectrum including continuous and discrete components by NFT. Critically, NFT aims at integrable conservative Hamiltonian models. Recent researches suggest that NFT can also characterize solitons in dissipative nonintegrable systems, which is regarded as perturbed NLSEs [26,29]. According to the distinct eigenvalue distributions of solitons and background, we can reconstruct the PS by separating the soliton eigenvalue from others. Thus in the perspective of the frequency domain, NFT could be a promising method to filter out the resonant sidebands in a dispersion-managed cavity. Referring to related works in mode-locked fiber lasers [22], we call this process CS distillation in passive Kerr resonators. We note that although CS

*These authors contributed equally to this work.
†wuzhichao@cug.edu.cn

formation has similarities to soliton mode locking in fiber lasers, it does not require additional saturable absorbers to stabilize them, and they differ fundamentally because the pump laser frequency is a part of the soliton spectrum. The external coherent pump provides a central control parameter of the soliton and in addition constitutes one of the comb lines which has no counterpart in conventional mode-locked lasers [30]. Therefore, it is deserved to investigate soliton distillation based on CSs.

Based on this process, we report on the CS distillation in a dispersion-managed Kerr resonator. In a longitudinally homogeneous resonator made of a uniform single-mode fiber (SMF), CSs can be successfully separated from the Kelly-like sidebands by NFT. In the case of a dispersion-managed cavity consisting of SMF and dispersion-shifted fiber (DSF), we can achieve CS distillation according to the eigenvalue distributions. Besides the spectrum filtering, we observe the characteristics of Kelly sidebands concerning detuning and net dispersion from the nonlinear spectrum, which could be utilized in analyzing specific nonlinear states in the future. On the one hand, we numerically demonstrate a feasible way for spectrum filtering in the passive Kerr cavity. On the other hand, our work can be a complementary part for understanding PSs in dissipative systems.

II. THEORETICAL MODEL

According to the experimental setup depicted in Ref. [20], we consider a dispersion-managed fiber ring resonator with a total length of 95 m consisting of the SMF and DSF. To precisely describe CSs in the longitudinally nonuniform cavity and the sidebands, we choose the infinite-dimensional Ikeda map to run the following simulations:

$$\frac{\partial E(z,\tau)}{\partial z} = -i\frac{\beta_2}{2}\frac{\partial^2 E(z,\tau)}{\partial \tau^2} + i\gamma|E(z,\tau)|^2 E(z,\tau), \quad (1)$$

$$E^{(m+1)}(0,\tau) = \sqrt{\theta}E_{\text{in}} + \sqrt{1-\rho}E^{(m)}(z,\tau)e^{-i\delta_0}, \quad (2)$$

where z is the longitudinal coordinate along the resonator, τ is the fast time in a reference frame moving with the intracavity field, and m is the round-trip index. γ and β_2 are Kerr nonlinear coefficient and group velocity dispersion (GVD), respectively. θ is the power coupling coefficient of the coupler and $\rho = 0.123$ is the fractional power loss per round trip including coupling loss and splicing loss between SMF and DSF segments. δ_0 is round-trip phase detuning between the pump frequency ω_p and resonance frequency ω_0, defined as $\delta_0 = (\omega_0 - \omega_p)\tau_R$. L is the total cavity length; τ_R is the round-trip time whose inverse is the free spectral range. E_{in} is the pump amplitude, thus P_{in} is the injected pump power. Here, Eq. (1) is the well-known NLSE which describes the evolution of the slowly varying electric field envelope $E^{(m)}(z,\tau)$ over a single round trip inside the cavity, while Eq. (2) describes the coherent injection of the driving field into the resonator. When combining the two equations, we can obtain a full map equation by inducing a Dirac function $\delta(\cdot)$ to express the periodic boundary condition [31],

$$\frac{\partial E(z,\tau)}{\partial z} + i\frac{\beta_2}{2}\frac{\partial^2 E(z,\tau)}{\partial \tau^2} - i\gamma|E|^2 E = \sum_{n=-\infty}^{+\infty}\delta(z-nL)[(1-\sqrt{1-\rho})E - \sqrt{\theta}E_{\text{in}}]. \quad (3)$$

The right-hand side of Eq. (3) can be regarded as a kind of periodically recurring function in z as reported in Ref. [25]. Then the CSs in the passive Kerr cavity are stationary solutions of the perturbed NLSE, which can be decomposed into nonlinear spectral data. As for the generalized NLSE, we achieve this process through the solution of a linear scattering problem, known as the Zakharov-Shabat problem (ZSP) [28]. The NFT is calculated from specific solutions of the ZSP:

$$\frac{d}{dt}\begin{pmatrix} v_1(t,\lambda) \\ v_2(t,\lambda)\end{pmatrix} = \begin{pmatrix} -j\lambda & E(t) \\ -E^*(t) & j\lambda\end{pmatrix}\begin{pmatrix} v_1(t,\lambda) \\ v_2(t,\lambda)\end{pmatrix}, \quad (4)$$

where $j^2 = -1$. $E(\tau)$ is the temporal waveform of CS calculated from Eqs. (1) and (2) (in normalized units [25]) and λ is a spectral parameter, which plays the role of a nonlinear analog of frequency. $v_{1,2}$ are auxiliary functions and the scattering data $a(\lambda)$ and $b(\lambda)$ can be calculated from them:

$$a(\lambda) = \lim_{t\to\infty} v_1(t,\lambda)e^{j\lambda t}, \quad b(\lambda) = \lim_{t\to\infty} v_2(t,\lambda)e^{-j\lambda t}. \quad (5)$$

Then the nonlinear spectrum of signal $E(\tau)$ is defined as

$$\tilde{E}_c(\lambda) = b(\lambda)/a(\lambda), \quad \lambda \in R,$$
$$\tilde{E}_d(\lambda) = b(\lambda_n)/a'(\lambda_n), \quad \lambda_n \in C^+. \quad (6)$$

$\tilde{E}_c(\lambda)$ is the continuous part of the nonlinear spectrum, which refers to the radiation component and converges to the ordinary Fourier spectrum at the low-power limit, and $\tilde{E}_d(\lambda_n)$ is the discrete part corresponding to the soliton component of the signal. λ_n is the eigenvalue in the upper half complex plane, which is defined as

$$a'(\lambda_n) = \left.\frac{da(\lambda)}{d\lambda}\right|_{\lambda=\lambda_n} = 0. \quad (7)$$

III. RESULTS AND DISCUSSIONS

We first consider a uniform cavity (SMF only, $L = 95$ m and $\beta_{2,\text{SMF}} = -21.2\times10^{-27}$ s^2/m), and compare the temporal waveforms and the corresponding spectra before and after NFT. The pump power P_{in} and the detuning δ_0 are set to be 5 W and 2.5 rad, respectively. Here, we normalize time to a scale $T_s = 4$ ps. Also, the amplitude is normalized with a scale Q_s, which is the squared root of the power of a hyperbolic secant signal with a time width equal to a time window containing 99% of the pulse energy. As can be seen in Fig. 1(a), a stable CS sits atop a resonant CW background with a series of weak perturbed waves. In the frequency domain, these perturbations correspond to the Kelly-like sidebands depicted in Fig. 1(b). When the CS is mapped into a nonlinear discrete spectrum by NFT, the eigenvalue corresponding to a PS has a large imaginary part (λ_I) related to the pulse amplitude and almost zero real part (λ_R) indicating that the PS has zero frequency drift. We note that, besides the eigenvalue of PS, other eigenvalues at the bottom of Fig. 1(c) have zero

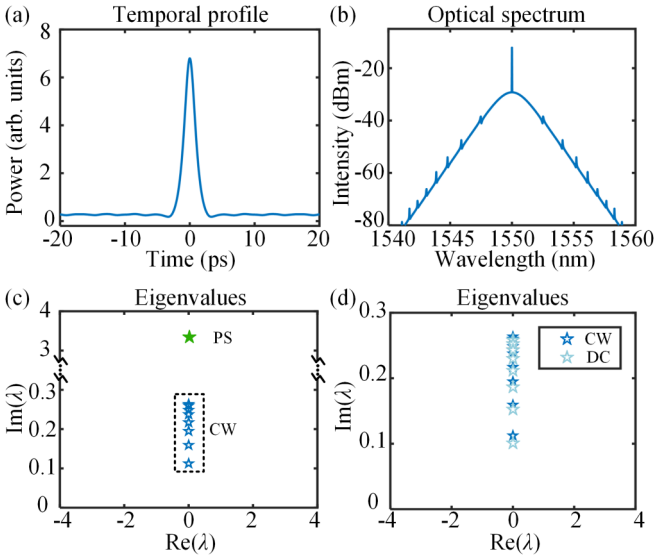

FIG. 1. (a) Temporal profile of the CS in the uniform cavity. (b) The corresponding spectrum of the CS in (a). (c) The nonlinear discrete spectrum of the CS. Green pentagram: the eigenvalue of PS; dark-blue hollow pentagrams: the eigenvalues of CW. (d) The eigenvalues at the bottom of (c) and our constructed direct-current component. Light-blue hollow pentagrams: the eigenvalues of dc.

real parts and weak imaginary parts, indicating weak amplitude and zero drifting velocity of the corresponding temporal components. We construct a direct-current component with a power of 0.26 W according to Fig. 1(a), and the corresponding discrete spectrum is illustrated as the light-blue pentagrams in Fig. 1(d), which almost coincide with those of the CS [dark-blue pentagrams in Fig. 1(d)]. Our numerical results demonstrate that these eigenvalues correspond to the CW base. The weak Kelly sidebands still locate at the nonlinear continuous spectrum because of the low-power limit. Similar to the soliton distillation process in the mode-locked fiber laser, we filter out the eigenvalues of the resonant CW background and reserve the eigenvalue of the PS. Then the true temporal waveform of PS can be obtained by the inverse NFT shown as the orange curve in Fig. 2(a) [25,32]:

$$q(t) = -2j\lambda_I \mathrm{sech}[2\lambda_I(\tau - \tau_0)]e^{-j[2\lambda_R\tau+\phi(z)]}, \qquad (8)$$

where $\phi(z)$ is the spectrum phase, and τ_0 is the time center associated with (λ_I) and spectrum amplitude. As is depicted in Fig. 2(b), the corresponding spectrum without any CW or

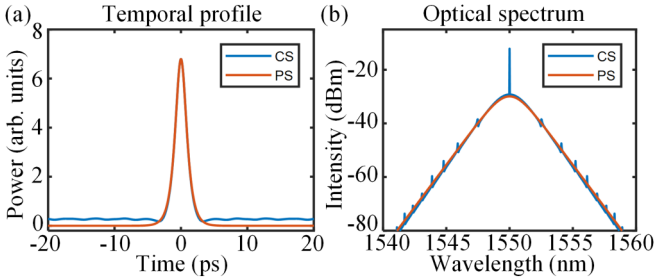

FIG. 2. (a) Temporal profiles of the CS and the distilled pure soliton. (b) Corresponding spectra of the temporal waveforms in (a).

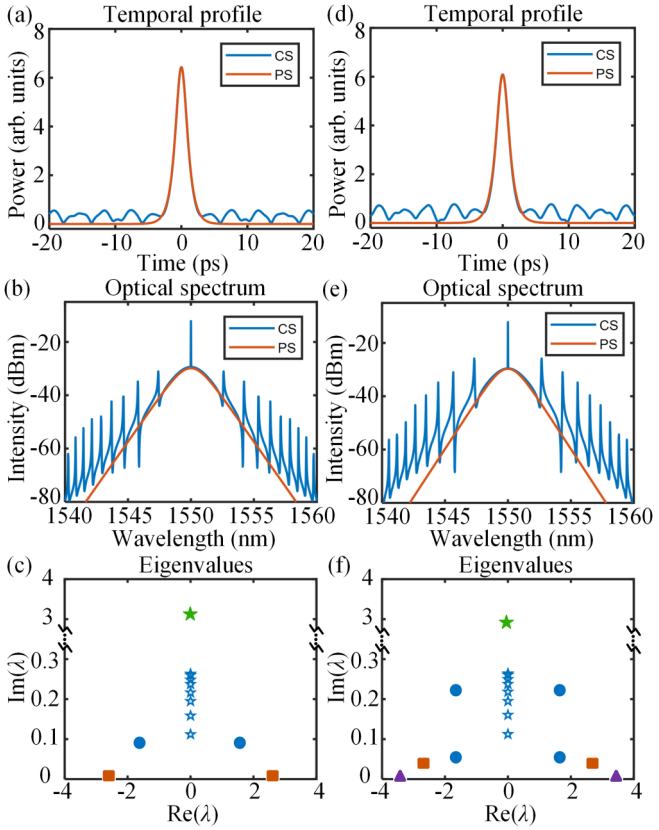

FIG. 3. (a), (d) Temporal profiles of CSs (blue curves) and distilled pure solitons (orange curves) when DSF = 5 and 10 m, respectively. (b), (e) Corresponding spectra of the temporal waveforms in (a) and (d). (c), (f) Nonlinear discrete spectra of CS in (a) and (d). Green pentagram: the eigenvalue of PS; dark-blue hollow pentagrams: the eigenvalues of CW; blue circles: the eigenvalues of the first-order sideband; orange squares: the eigenvalues of the second-order sideband; purple triangles: the eigenvalues of the third-order sideband.

sideband components has a sech^2 shape, which indicates the soliton distillation also works for the CS in the passive Kerr resonator.

Then we concentrate on the characteristics of the CS in the dispersion-managed cavity. Fixing the detuning δ_0 and the total cavity length L to be 2.5 rad and 95 m, respectively, we display the simulated temporal waveforms and spectra at two different lengths of DSF ($\beta_{2,\mathrm{SMF}} = 2\times10^{-27}$ s^2/m), as shown in Fig. 3. With 5-m-long DSF, the amplitude of the resonant CW background shown in Fig. 3(a) is significantly enhanced compared to that in the uniform cavity [cf. Fig. 1(a)], which is predominantly affected by the periodic variation of the cavity dispersion. The amplitude of the corresponding sidebands is also increased as is shown in Fig. 3(b). The peak of the CS is a little bit decreased due to the power conversion to the sidebands, which acts as a nonlinear loss mechanism. When the CS is mapped to the nonlinear discrete spectrum, the principal characteristics (intensity and frequency) are reserved including PS, CW background, and first- and second-order sidebands. The PS illustrated as the orange curves in Figs. 3(a) and 3(b) is successfully distilled

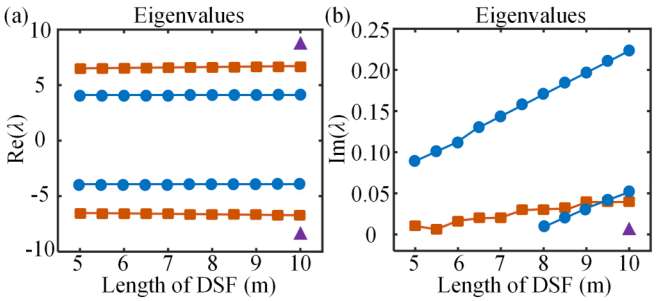

FIG. 4. (a), (b) The real and imaginary parts of the eigenvalues corresponding to the Kelly-like sidebands vary with the length of DSF.

by filtering out the eigenvalues of the CW background and the sidebands. With increasing the length of DSF to 10 m, the intensity of the sidebands [Fig. 3(e)] is further enhanced with indistinguishable variations of frequency position. These features are also displayed clearly in the discrete spectra shown in Figs. 3(c) and 3(f). The net cavity GVD $\langle\beta_2\rangle$ in the two cases (DSF = 5 m and DSF = 10 m) is -19.98×10^{-27} s^2/m and -18.76×10^{-27} s^2/m, respectively. According to the phase-matching condition [20] $\langle\beta_2\rangle/2(\omega-\omega_0)^2L = 2\pi n + \delta_0$, the frequency variation of the sidebands is very small, which is consistent with the results shown in the discrete spectra. More detailed variations of the sideband eigenvalues are shown in Fig. 4; the sidebands not showing up are retained in the continuous spectrum due to their lower intensity. The real parts of different order sidebands all locate at the horizontal lines indicating constant frequency position. The imaginary parts increase with the length of DSF indicating intensity enhancement. Thus, considering the perspective of the nonlinear spectrum, the intensities of the Kelly-like sidebands can be magnified by the dispersion management without significant position variations. Detuning is another physical parameter that can affect the characteristics of CS [3]. Here, we investigate the simulated CSs at the detunings of 2.3 and 3.6 rad, respectively. Comparing the results shown in Figs. 5(a) and 5(d), detuning can significantly increase the peak power of the soliton. At the frequency domain, the resonant radiation sidebands drift toward the pump frequency and grow in intensity with increasing detuning. The related phenomena can be observed in the nonlinear discrete spectra by the variation of eigenvalues distribution [Figs. 5(c) and 5(f)]. More detailed variations of the sideband eigenvalues are depicted in Fig. 6. The real parts of different order sidebands decrease with the detuning indicating their approaching the spectrum center. The imaginary parts increase with the detuning indicating intensity amplification. For the dispersion-managed cavity, the main time-frequency features of CSs are illustrated in a single nonlinear discrete spectrum. Therefore, NFT can be an effective analyzing method for the CSs with complex sidebands.

The Kelly-like sidebands here are perfectly symmetric concerning the pump line. We extend the distillation method to the case of asymmetric sidebands such as Cherenkov radiation (the dispersive wave). We assume a third-order dispersion (TOD = 10^{-38} s^3/m) in the longitudinally homogeneous cavity. Figure 7(d) shows the temporal evolution of the CS in the cavity. Intercepting one round trip, we can see that the

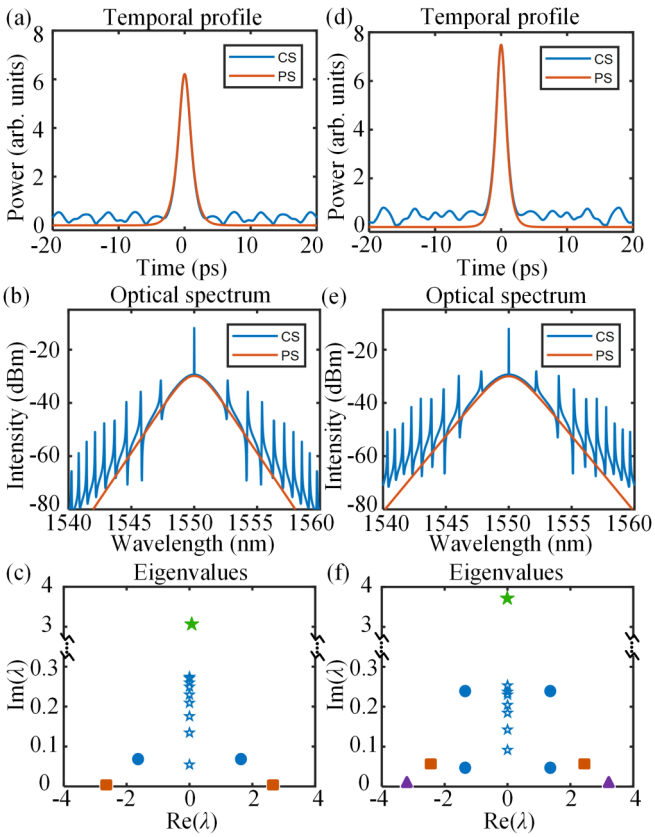

FIG. 5. (a), (d) Temporal profiles of CSs (blue curves) and distilled pure solitons (orange curves) when $\delta_0 = 2.3$ and 3.6 rad, respectively. (b), (e) Corresponding spectra of the temporal waveforms in (a) and (d). (c), (f) Nonlinear discrete spectra of CS in (a) and (d).

amplitude of the resonant CW background on the right side of CS is much larger than that on the left [Fig. 7(a)]. An asymmetric sideband locates at a longer wavelength and there is a spectrum recoil resistant to the strong dispersive wave [Fig. 7(b)]. In the nonlinear spectrum shown in Fig. 7(c), the dispersive wave is mapped to the eigenvalue with real part of 15. The eigenvalue of the CS has a distinguishable real part indicating a frequency drift corresponding to the spectrum recoil. Thus the reconstructed PS shown in Fig. 7(e) has the same temporal drifting velocity as the undistilled CS.

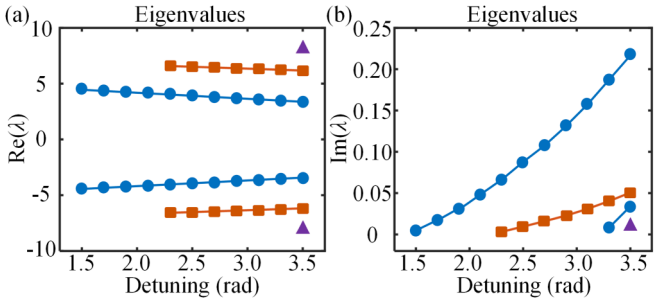

FIG. 6. (a), (b) The real and imaginary parts of the eigenvalues corresponding to the Kelly-like sidebands vary with the detuning.

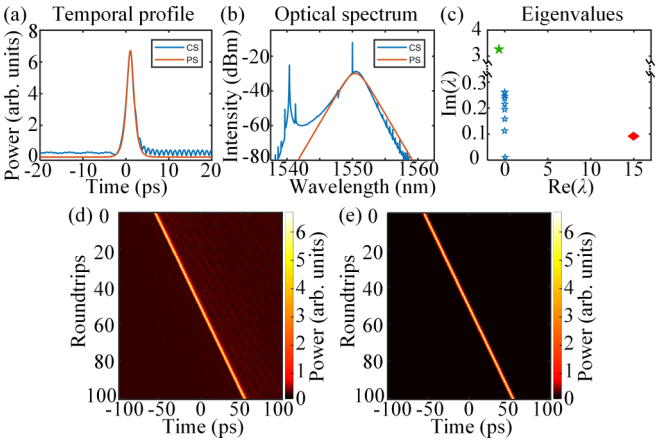

FIG. 7. (a) Temporal profiles of the CS with TOD (blue curves) and the distilled PS (orange curves). (b) Corresponding spectra of the temporal waveforms in (a). (c) The nonlinear discrete spectrum of the CS in (a). Green pentagram: the eigenvalue of PS; dark-blue hollow pentagrams: the eigenvalues of CW; red diamond: the eigenvalue of the dispersive wave. (d), (e) The temporal evolutions of the CS and the distilled PS, respectively.

IV. CONCLUSIONS AND DISCUSSIONS

In summary, we report on the soliton distillation in the dispersion-managed passive Kerr resonator based on the NFT algorithm. According to the distinct eigenvalue distributions of CS, CW background, and resonant radiation sidebands, a PS can be successfully reconstructed by inverse NFT. We also investigate the position and intensity of these sidebands changing with the length of DSF and detuning. In addition to the symmetric sidebands, this CS distillation process is also demonstrated to be suitable for the asymmetric condition such as dispersive wave induced by TOD. Our calculations indicate that a nonlinear spectrum can reserve the notable features both in the time and frequency domains, which is conducive to the overall analysis.

To date, the bright dissipative solitons investigated in the passive Kerr resonator are hyperbolic secant temporal pulses. The soliton sustained by the dispersion-managed cavity with the near-zero net cavity dispersion is demonstrated to have a Gaussian profile [20]. A dispersive wave due to third-order dispersion is also observed in its spectrum. In addition, CSs in the uniform near-zero dispersive cavity are also theoretically and experimentally demonstrated [33]. The asymmetric dispersive waves induced by the high-order dispersion show up in the spectrum. Further NFT-based study in these conditions can be helpful in understanding the characteristics of the near-zero solitons and achieving the spectral shaping. In the experimental aspect, the dual-comb-based asynchronous optical sampling can be a promising method in obtaining the full-field information. To ensure the sampling precision and coherence, a controllable polarization-multiplexed scalar soliton can be generated in a single cavity as the dual-comb source [34]. The present work can pave the way for the soliton investigation by NFT in a dissipative nonlinear system.

ACKNOWLEDGMENTS

We acknowledge the support from the Open Project Program of Wuhan National Laboratory for Optoelectronics (Grant No. 2019WNLOKF005); the Natural Science Foundation of Hubei Province (Grants No. 2019CFB598 and No. 2020CFB440); the National Natural Science Foundation of China (Grants No. 61605179 and No. 62005255); and the Fundamental Research Funds for the Central Universities, China University of Geosciences (Wuhan) (Grants No. 1910491B06, No. ZL201917, No. G1320311998, and No. 162301192695).

[1] T. J. Kippenberg, A. L. Gaeta, M. Lipson, and M. L. Gorodetsky, Dissipative Kerr solitons in optical microresonators, Science **361**, 6402 (2018).

[2] T. J. Kippenberg, R. Holzwarth, and S. A. Diddams, Microresonator-based optical frequency combs, Science **332**, 6029 (2011).

[3] T. Herr, V. Brasch, J. D. Jost, C. Y. Wang, N. M. Kondratiev, M. L. Gorodetsky, and T. J. Kippenberg, Temporal solitons in optical microresonators, Nat. Photon. **8**, 145 (2014).

[4] F. Leo, S. Coen, P. Kockaert, S.-P. Gorza, P. Emplit, and M. Haelterman, Temporal cavity solitons in one-dimensional Kerr media as bits in an all-optical buffer, Nat. Photon. **4**, 7 (2010).

[5] V. Brasch, M. Geiselmann, T. Herr, G. Lihachev, M. H. P. Pfeiffer, M. L. Gorodetsky, and T. J. Kippenberg, Photonic chip-based optical frequency comb using soliton Cherenkov radiation, Science **351**, 6271 (2016).

[6] B. Stern, X. C. Ji, Y. Okawachi, A. L. Gaeta, and M. Lipson, Battery-operated integrated frequency comb generator, Nature (London) **562**, 7727 (2018).

[7] C. Monat, C. Grillet, M. Collins, A. Clark, J. Schroeder, C. Xiong, J. Li, L. O'Faolain, T. F. Krauss, B. J. Eggleton, and D. J. Moss, Integrated optical auto-correlator based on third-harmonic generation in a silicon photonic crystal waveguide, Nat. Commun. **5**, 3246 (2014).

[8] P. Trocha, M. Karpov, D. Ganin, M. H. P. Pfeiffer, A. Kordts, S. Wolf, J. Krockenberger, P. Marin-Palomo, C. Weimann, S. Randel, W. Freude, T. J. Kippenberg, and C. Koos, Ultrafast optical ranging using microresonator soliton frequency combs, Science **359**, 6378 (2018).

[9] M.-G. Suh and K. J. Vahala, Soliton microcomb range measurement, Science **359**, 6378 (2018).

[10] S. Diallo and Y. K. Chembo, Optimization of primary Kerr optical frequency combs for tunable microwave generation, Opt. Lett. **42**, 18 (2017).

[11] X. Xue, Y. Xuan, H.-J. Kim, J. Wang, D. E. Leaird, M. Qi, and A. M. Weiner, Programmable single-bandpass photonic RF filter based on Kerr comb from a microring, J. Lightwave Technol. **32**, 20 (2014).

[12] E. Obrzud, M. Rainer, A. Harutyunyan, M. H. Anderson, J. Q. Liu, M. Geiselmann, B. Chazelas, S. Kundermann, S. Lecomte, M. Cecconi, A. Ghedina, E. Molinari, F. Pepe, F. Wildi, F. Bouchy, T. J. Kippenberg, and T. Herr, A microphotonic astrocomb, Nat. Photon. **13**, 31 (2019).

[13] M.-G. Suh, X. Yi, Y.-H. Lai, S. Leifer, I. S. Grudinin, G. Vasisht, E. C. Martin, M. P. Fitzgerald, G. Doppmann, J. Wang, D. Mawet, S. B. Papp, S. A. Diddams, C. Beichman, and K. Vahala, Searching for exoplanets using a microresonator astrocomb, Nat. Photon. **13**, 25 (2019).

[14] M. G. Suh, Q. F. Yang, K. Y. Yang, X. Yi, and K. J. Vahala, Microresonator soliton dual-comb spectroscopy, Science **354**, 6312 (2016).

[15] A. Dutt, C. Joshi, X. Ji, J. Cardenas, Y. Okawachi, K. Luke, A. L. Gaeta, and M. Lipson, On-chip dual-comb source for spectroscopy, Sci. Adv. **4**, 3 (2018).

[16] K. Tamura, E. P. Ippen, H. A. Haus, and L. E. Nelson, 77-fs pulse generation from a stretched-pulse mode-locked all-fiber ring laser, Opt. Lett. **18**, 13 (1993).

[17] H. A. Haus, K. Tamura, L. E. Nelson, and E. P. Ippen, Stretched-pulse additive pulse mode-locking in fiber ring lasers: Theory and experiment, IEEE J. Quantum Electron. **31**, 591 (1995).

[18] C. Bao and C. Yang, Stretched cavity soliton in dispersion-managed Kerr resonators, Phys. Rev. A **92**, 023802 (2015).

[19] X. Dong, Q. Yang, C. Spiess, V. G. Bucklew, and W. H. Renninger, Stretched-Pulse Soliton Kerr Resonators, Phys. Rev. Lett. **125**, 033902 (2020).

[20] A. U. Nielsen, B. Garbin, S. Coen, S. G. Murdoch, and M. Erkintalo, Emission of intense resonant radiation by dispersion-managed Kerr cavity solitons, APL Photon. **3**, 12 (2018).

[21] A. F. J. Runge, C. Aguergaray, N. G. R. Broderick, and M. Erkintalo, Coherence and shot-to-shot spectral fluctuations in noise-like ultrafast fiber lasers, Opt. Lett. **38**, 21 (2013).

[22] Y. Wang, S. Fu, C. Zhang, X. Tang, J. Kong, J. H. Lee, and L. Zhao, Soliton distillation of pulses from a fiber laser, J. Lightwave Technol. **39**, 8 (2021).

[23] Y. Wang, S. Fu, J. Kong, A. Komarov, M. Klimczak, R. Buczyski, X. Tang, M. Tang, Y. Qin, and L. Zhao, Nonlinear Fourier transform enabled eigenvalue spectrum investigation for fiber laser radiation, Photon. Res. **9**, 8 (2021).

[24] P. Ryczkowski, M. Narhi, C. Billet, J. M. Merolla, G. Genty, and J. M. Dudley, Real-time full-field characterization of transient dissipative soliton dynamics in a mode-locked laser, Nat. Photon. **12**, 221 (2018).

[25] S. Sugavanam, M. K. Kopae, J. Peng, J. E. Prilepsky, and S. K. Turitsyn, Analysis of laser radiation using the nonlinear Fourier transform, Nat. Commun. **10**, 5663 (2019).

[26] S. K. Turitsyn, I. S. Chekhovskoy, and M. P. Fedoruk, Nonlinear Fourier transform for characterization of the coherent structures in optical microresonators, Opt. Lett. **45**, 11 (2020).

[27] L. D. Faddeev and L. A. Takhtajan, *Hamiltonian Methods in the Theory of Solitons* (Springer-Verlag, Berlin, 2007).

[28] V. E. Zakharov and A. B. Shabat, Exact theory of two-dimensional self-focusing and one-dimensional self-modulation of waves in nonlinear media, J. Exp. Theor. Phys. **34**, 1 (1972).

[29] S. K. Turitsyn, I. S. Chekhovskoy, and M. P. Fedoruk, Nonlinear Fourier transform for analysis of optical spectral combs, Phys. Rev. E **103**, L020202 (2021).

[30] M. E. Fermann and I. Hartl, Ultrafast fibre lasers, Nat. Photon. **7**, 1006 (2013).

[31] X. Xue, X. Zheng, and B. Zhou, Super-efficient temporal solitons in mutually coupled optical cavities, Nat. Photon. **13**, 616 (2019).

[32] M. I. Yousefi and F. R. Kschischang, Information transmission using the nonlinear Fourier transform, part I: Mathematical tools, IEEE Trans. Inf. Theory **60**, 7 (2014).

[33] Z. Li, Y. Xu, S. Coen, S. G. Murdoch, and M. Erkintalo, Experimental observations of bright dissipative cavity solitons and their collapsed snaking in a Kerr resonator with normal dispersion driving, Optica **7**, 9 (2020).

[34] J. Pan, Z. Cheng, T. Huang, M. Zhu, Z. Wu, and P. P. Shum, Numerical investigation of all-optical manipulation for polarization-multiplexed cavity solitons, J. Lightwave Technol. **39**, 2 (2021).